DIRECT NUMERICAL SIMULATION OF COMPRESSIBLE SHEAR LAYER WITH HEAT SOURCE

Sandro F. Quirino, fonsecaquirino@yahoo.com.br
Instituto Nacional de Pesquisas Espaciais—INPE
Márcio T. Mendonça, marcio@iae.cta.br
Comando Geral de Tecnologia Aeroespacial, Instituto de Aeronáutica e Espaço—CTA/IAE

Abstract. *In this work Direct Numerical Simulation of compressible, subsonic mixing layers with heat source is performed in a two-dimensional temporal analysis. The heat source is a simplified model of a reacting flow. The simulation considers the temporal evolution of an initial laminar shear layer, where disturbances are amplified forming the characteristic vortices of a Kelvin-Helmholtz instability. The Navier-Stokes are solved numerically using compact, high-order finite differences for the spatial derivatives and a 4^{th} Runge-Kutta scheme for the temporal terms. The results show that the combination of heat addition and compressibility reduces significantly the amplification of disturbances and the range of wavenumbers that are unstable, delaying the transition to a turbulent regime and contributing negatively for the process of mixture of fluids in the mixing layer.*

Keywords: *shear layer stability, compressible flow stability, Kelvin-Helmholtz stability, direct numerical simulations*

1. INTRODUCTION

In propulsive systems, combustion efficiency and the exhaust of pollutants to the atmosphere are directly related to the quality of the air-fuel mixing. Fuel consumption and the exhaust of carbon monoxide, unburned hydrocarbons and nitric oxides have to be minimized. Usually in diffusive flames turbulence is a desired characteristic of the flow due to its higher diffusive proprieties, which allows a better mixing between the reactants. Nevertheless, in supersonic combustion, which is sought for hypersonic flight, turbulence is stabilized and laminar flows are much more stable due to compressibility effects. The end result is that diffusion flames, that depend strongly on turbulence for the effective mixing of fuel and oxidizer may not be an effective process in the compressible regime. A mixing layer or shear layer is the simples model for the interface in a binary fuel-oxidizer system as shown in Fig. 1. The predominant instability in the shear layer is inviscid according to Rayleigh's and Fjortoft inflection point theorem.

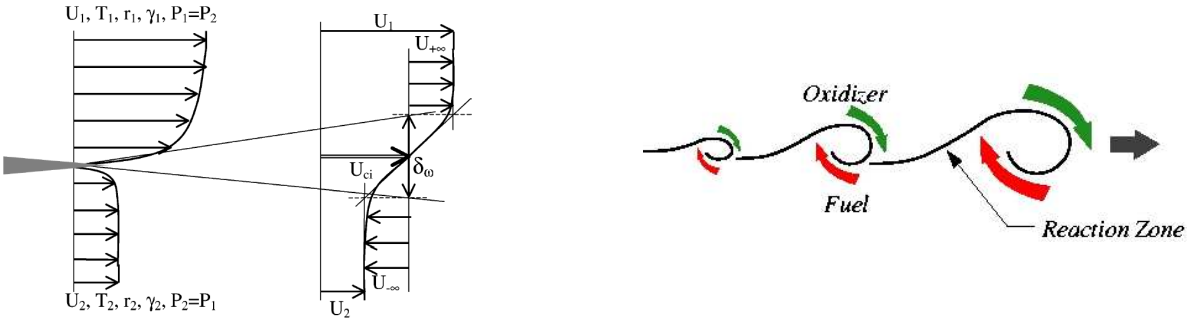

Figure 1. Fuel-oxidizer interface in a shear layer.

The process by which fuel and oxidizer are mixed in a shear layer was identified by Brown and Roshko, 1974. The typical Kelvin-Helmholtz instability structures provide two mixing mechanisms, one due to entrainment on the large scale structures and the other by vortex pairing. the second is the most important, since the large scale vortical structures may move large quantities of reactants without mixing. Ho and Huerre, 1984 present a detailed review of experimental and numerical references on shear layer stability. For incompressible and moderately compressible flows a single vortical structures is formed as shown in Fig. 1. Increasing compressibility has a stabilizing effect on the shear layer and the amplification rates are reduced with increasing convective Mach number as reported by Lessen et al., 1965; Lessen et al., 1966; Groppengiesser, 1970; Chinzei et al., 1986; Papamoschou and Roshko, 1988 and Clemens and Mungal, 1995. These previous works also identified that increased compressibility results in three-dimensional modes that have a higher amplification rate than two-dimensional modes.

Compressibility has also a third effect, that results in the development of two unstable modes, called external modes, as identified by Jackson and Grosch, 1989 and Jackson and Grosch, 1990. These modes have amplitude peaks out of the shear layer centre line, resulting in the structure shown in Fig. 2. High convective Mach number shear layers in reacting systems have higher instability amplification rates for the external modes compared to the central mode. The mixing

process becomes a two step process in this case. Further investigations confirmed the existence and higher growth rate of the external modes when combustion is considered as reported by Planché, 1993; Shin and Ferziger, 1991; Shin and Ferziger, 1993 and Planché, 1993.

As a result of these investigations important conclusions were drawn. First the laminar velocity profile used in stability analysis has a large influence on the results, as well as the consideration of variable gas properties such as viscosity and density, according to Shin and Ferziger, 1991 and Shin and Ferziger, 1993. Second incompressible flows with combustion reaction also result in large amplification rates for the external modes, but a predominance of two-dimensional disturbances, unlike compressible flows with high Mach number, for which three-dimensional disturbances have a higher growth rate.

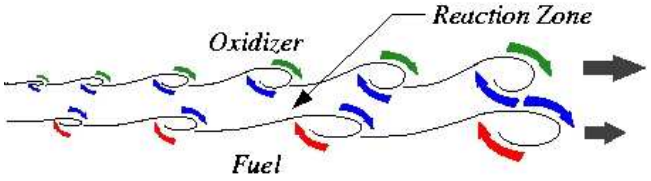

Figure 2. Development of external modes in compressible and reacting shear layers.

Based on these previous conclusions Day et al., 1998 and Day et al., 2001 presented numerical results with a broader range of parameters, including nonlinear effects up to the secondary instability regions. These works considered linear stability analysis, parabolized stability equations and direct numerical simulations. Other direct numerical simulations were performed by Sauvage and Kourta, 1999; Sandham and Reynolds, 1991 and Germanos and Medeiros, 2005. The last two without chemical reaction.

In this work the compressible Navier-Stokes equations are solved numerically including an internal heat source in the energy equation. This heat source simulates the effect of a combustion reaction. Only the initial linear stages of Kelvin-Helmholtz instability are simulated. Therefore, the two-dimensional Navier-Stokes suffice to capture the variation of amplification rate with heat source strength and compressibility.

2. GOVERNING EQUATIONS AND NUMERICAL METHOD

The governing equations are the two-dimensional compressible Navier-Stokes equations in a Cartesian coordinate system given in non-dimensional form by:

$$\frac{\partial \rho}{\partial t} + \frac{\partial (\rho u)}{\partial x} + \frac{\partial (\rho v)}{\partial y} = 0, \tag{1}$$

$$\frac{\partial \rho u}{\partial t} + \frac{\partial}{\partial x}(\rho u^2 + p - \tau_{xx}) + \frac{\partial}{\partial y}(\rho uv - \tau_{xy}) = 0, \tag{2}$$

$$\frac{\partial \rho v}{\partial t} + \frac{\partial}{\partial y}(\rho v^2 + p - \tau_{yy}) + \frac{\partial}{\partial x}(\rho uv - \tau_{xy}) = 0, \tag{3}$$

$$\frac{\partial E_t}{\partial t} + \frac{\partial}{\partial x}[(E_t + p)u + q_x - u\tau_{xx} - v\tau_{xy}] + \frac{\partial}{\partial y}[(E_t + p)v + q_y - u\tau_{xy} - v\tau_{yy}] + Q = 0. \tag{4}$$

Where ρ is the fluid density, u and v are the velocities in the streamwise x and normal y directions, t is the time and p the static pressure and Q a heat source. The components of the stress tensor τ and heat fluxes q are given by:

$$\tau_{xy} = \frac{\mu}{Re}\left(4\frac{\partial u}{\partial y} - 2\frac{\partial v}{\partial x}\right), \quad \tau_{xx} = \frac{\mu}{3Re}\left(4\frac{\partial u}{\partial x} - 2\frac{\partial v}{\partial y}\right), \quad \tau_{yy} = \frac{\mu}{3Re}\left(4\frac{\partial v}{\partial y} - 2\frac{\partial u}{\partial x}\right). \tag{5}$$

$$q_x = \frac{-\mu}{(\gamma - 1)M^2 PrRe}\frac{\partial T}{\partial x}, \qquad q_y = \frac{-\mu}{(\gamma - 1)M^2 PrRe}\frac{\partial T}{\partial y}. \tag{6}$$

Where M, Pr and Re are the Mach, Prandtl and Reynolds numbers.

$$M = \frac{U}{a}, \qquad Pr = \frac{c_p \mu}{k}, \qquad Re = \frac{\rho U \delta_\omega}{\mu}, \tag{7}$$

The total energy E_t and the perfect gas relations are:

$$E_t = \rho\left(e + \frac{1}{2}u^2 + \frac{1}{2}v^2\right), \qquad de = c_v dT, \qquad p = \rho(\gamma - 1)e. \tag{8}$$

The dynamic viscosity variation with temperature follows a power law $\mu = \mu_o T^{0.65}$.

These governing equations in non-dimensional form have reference values given by the fast stream, such that the reference velocity and temperature are U_1 and T_1, the reference density and viscosity are ρ_1 and μ_1 and the length scale is the vorticity thickness based on the velocity U_{ci} at the point of inflection:

$$\delta_\omega = \frac{(U_1 - U_2)}{\left(\frac{dU_{ci}}{dy}\right)_{max}}, \tag{9}$$

2.1 Initial and Boundary Conditions

Initial conditions are given based on a periodic disturbance added to a laminar hyperbolic tangent profile for the streamwise velocity such that:

$$u_L(y) = \frac{(U_1 + U_2)}{2} + \frac{(U_1 - U_2)}{2}\tanh(\sigma y), \quad v_L(y) = 0, \quad T_L(y) = a + \frac{(1 - u_L(y))T_2}{(1 - U_2)} + \frac{u_L(y) - U_2}{(1 - U_2)}. \tag{10}$$

Where the subscript L stands for the laminar base flow and

$$a = \frac{(M_1)^2(\gamma - 1)}{2}\left[u_L(y)(1 - U_2) - (u_L)^2 - U_2)\right], \tag{11}$$

$$e_L(y) = \frac{T_L(y)\gamma(\gamma - 1)}{(M_1)^2}. \qquad \rho_L = \frac{P_L(y)}{e_L(y)(\gamma - 1)}, \qquad E_{tL} = \rho_L\left[e_L + \frac{(u_L(y)^2 + v_L(y)^2)}{2}\right]. \tag{12}$$

The Crocco-Bussemann relation was used to specify the initial temperature distribution

The initial disturbances are given by a periodic variation in the streamwise direction and an exponential decay in the normal direction:

$$u' = 2\sigma y e^{-(\sigma y^2)}\left[\frac{A_1\cos(\alpha_1 x)}{\alpha_1} + \frac{A_2\cos(\alpha_2 x)}{\alpha_2}\right], \qquad v' = e^{-(\sigma y^2)}\left[A_1\sin(\alpha_1 x) + A_2\sin(\alpha_2 x)\right]. \tag{13}$$

Where σ adjusts the disturbances thickness, A_1 e A_2 are amplitude related to the wavenumbers α_1 e α_2. The wavelength are $\lambda_1 = 2\pi/\alpha_1$ and $\lambda_2 = 2\pi/\alpha_2$. The disturbance velocities u' and v' are related by the incompressible continuity equation.

Far from the shear layer the flow is considered laminar and in the streamwise direction the disturbances are periodic with wavelength $L_x = \lambda$. For a variable ϕ:

$$\phi(y \to +\infty) = \phi_1, \qquad \phi(y \to -\infty) = \phi_2. \qquad \phi(x, y) = \phi(x + L_x, y). \tag{14}$$

Where the normal velocity components at $\pm\infty$ is zero and the initial pressure is uniform across the shear layer.

2.2 Numerical Method

The governing equations are solved numerically. By now, it is well known the advantages of high order compact schemes due to their higher performance regarding dissipation and dispersion errors according to Lele, 1992; Mahesh, 1998 and Souza, 2003. The equations are discretized using a 4th order Runge-Kutta for the temporal terms. The time step is limited in this explicit method and the following criterion was used, limiting the Courant number C to less then or equal to 1, Sandham, 1990:

$$dt = \frac{C}{\pi\left[\frac{1}{M_1}\left(\frac{1}{dx} + \frac{1}{dy}\right) + \left(\frac{|u|}{dx} + \frac{|v|}{dy}\right) + \frac{\mu}{\rho(\gamma-1)M_1^2 P_r R_e}\left(\frac{1}{dx} + \frac{1}{dy}\right)\right]} \tag{15}$$

Where dt is the time step, M_1 is the Mach number of the fast stream, Pr_{r1} and Re_1 are the reference Prandtl and Reynolds numbers, γ is the ratio of specific heats, dx and dy are the spacing in the streamwise and normal directions.

The spatial derivatives are discretized with 6th and 5th order compact finite differences. Interior points are discretized with the usual compact differences presented by Lele, 1992. Points at the upper and lower boundaries are discretized with an asymmetric 5th order stencil. Points neighboring the boundaries are discretized with a 6th order asymmetric stencil. These boundary and near boundary schemes are presented below and additional information can be found in Souza, 2003.

$$f_1' + 4f_2' = \frac{1}{24dx}(-74f_1 + 16f_2 + 72f_3 - 16f_4 + 2f_5) + 0(dx)^5 \tag{16}$$

$$f_1' + 6f_2' + 2f_3' = \frac{1}{120dx}(-406f_1 - 300f_2 + 760f_3 - 80f_4 + 30f_5 - 4f_6) + 0(dx)^6. \tag{17}$$

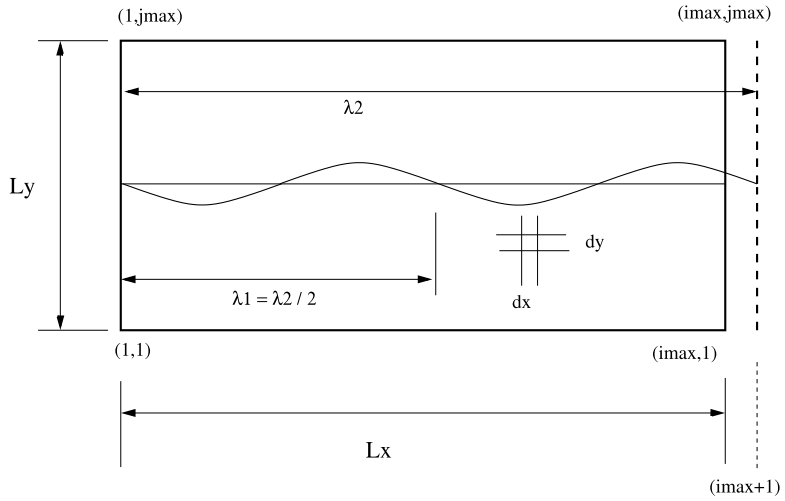

Figure 3. Domain

Second order derivatives are approximated by two consecutive first order stencils. Detail representation of the finite differences resulting matrices can be found in Quirino, 2006 due to size limitations in this article. The computational domain is represented in Fig. 3 containing a shear layer with vorticity thickness δ_ω defined in Eq. 9.

The computational grid in the normal direction has 10 to 18 times more grid points than the number of grid points in the streamwise direction, that has weaker gradients. No special consideration were given to avoid the reflexion of noise at the boundaries. In other words, non-reflexive boundary conditions were not implemented. In order to avoid the destruction of the numerical solution by noise reflection, the boundaries at the upper and lower boundaries had to be distanced from the shear layer. In certain cases the domain was more than one hundred times the shear layer vorticity thickness. Extensive numerical tests were performed for each test case presented in order to establish the adequate domain size and number of grid points.

2.3 Code Verification

Figure 4 presents comparisons between amplification rates versus wavenumber obtained with the present model against the numerical results from Sandham, 1990 for two compressibility levels $M = 0.4$ and $M = 0.8$. In the low wavenumber limit the code predicts amplification rates that are not in agreement with other results available in the literature. The reason for that is the inadequate choice of initial condition that are not based on linear stability analysis results. The initial conditions defined in 13 results in the growth of higher harmonics that prevails due to their higher amplification rates. The resulting vortex topology, given by vorticity iso-lines are in good agreement with results presented by Sandham, 1990 (not shown).

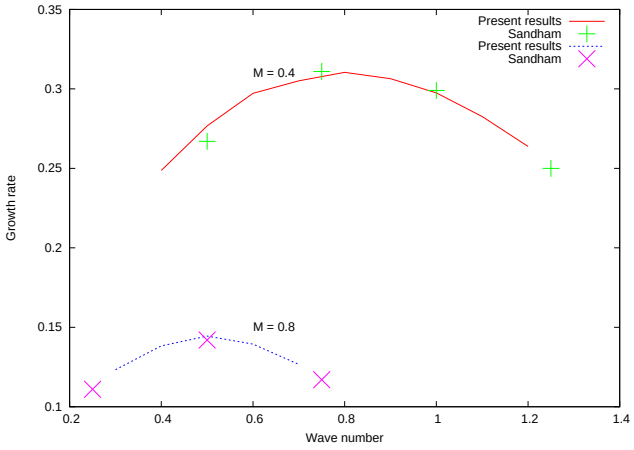

Figure 4. Amplification rate versus wavenumber for compressible shear layer without heat source. Comparison with numerical results from Sandham, 1990.

Amplification rates ω were measured based on the growth of the maximum normal velocity component:

$$\omega = \frac{v(t+dt) - v(t)}{dt\ v(t)}, \tag{18}$$

3. RESULTS

3.1 Compressibility Effects

According to previous studies discussed in the literature review presented above, compressibility is stabilizing and, therefore, has a negative effect on the mixing process in a binary fuel-oxidizer shear layer. Figure 5 shows the amplification rate versus wavenumber for three different values of Mach number. This figure shows not only that the amplification rates are reduced with increasing Mach number, but the range of wavenumbers that are amplified is reduced.

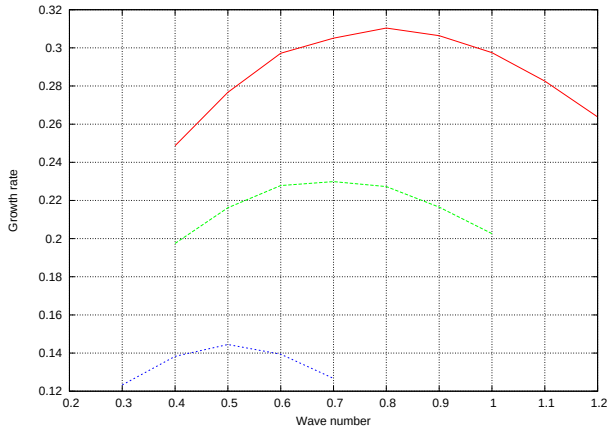

Figure 5. Amplification rate versus wavenumber for three different Mach numbers, $Ma = 0.4, 0.6$ and 0.8.

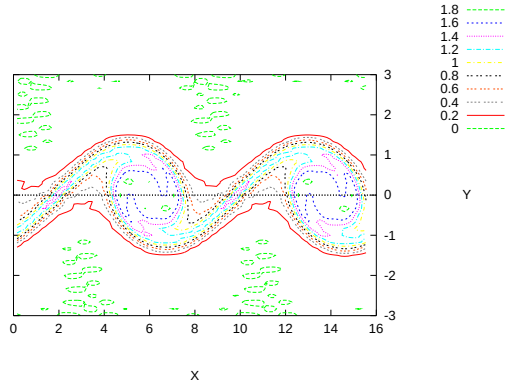

Figure 6. Vorticity iso-lines for $M = 0.4$ and $\alpha = 0.8$ at $t = 31.80$.

Figure 6, 7 and 8 show iso-vorticity lines for M =0.4, 0.6 and 0.8 respectively. These plots corresponds to the time close to the point where the vortices saturate. The wavenumber of each case corresponds to the one with the higher amplification rate for the given Mach number. The noise close to the boundaries are due to numerical reflection. The cortices are more or less elongated for different Mach numbers. The time taken to rich saturation is higher with increasing Mach number.

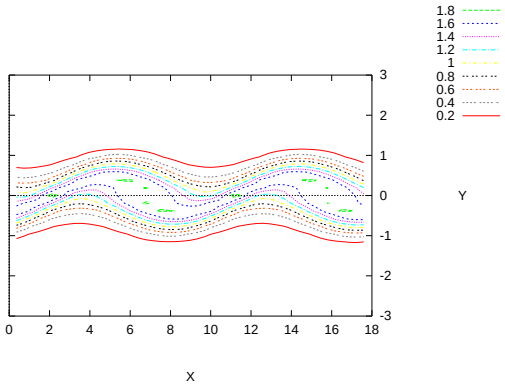

Figure 7. Vorticity iso-lines for $M = 0.6$ and $\alpha = 0.7$ at $t = 38.87$.

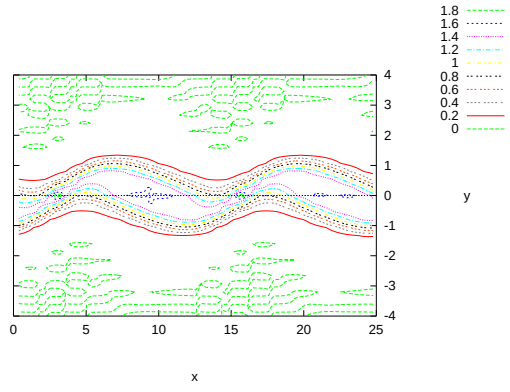

Figure 8. Vorticity iso-lines for $M = 0.8$ and $\alpha = 0.5$ at $t = 62.48$

3.2 Compressible Shear Layer With Heat Source

Adding a heat source to the energy equation, one can study the effect of heat addition on the stability of the compressible shear layer. The heat source has a Gaussian distribution $Q(y) = c\ e^{-\sigma y^2}$ centered at the shear layer, with a

thickness controlled by σ. Four different levels of heat were considered for each compressibility levels, $c_1 = 3,0 \cdot 10^{-3}$, $c_2 = 5,0 \cdot 10^{-3}$, $c_3 = 7,0 \cdot 10^{-3}$, $c_4 = 9,0 \cdot 10^{-3}$. Where c is the maximum amplitude of the source.

Figure 9 presents the amplification rate versus wavenumber for a shear layer with $M = 0.4$. The results show that the amplification rate is reduced due to heat addition. The amplification rates are reduced with the increase in the heat source strength. The wavenumber corresponding to the maximum amplification rate was not changed for the four heat source levels considered. The heat source inhibit the development of the vortices, having a similar effect of compressibility. The temporal evolution of the velocity normal component $v(t)$ is shown in Fig. 10 for $Ma = 0.4$ and wavenumber $\alpha = 0.8$. A initial numerical transient region is observed due to the specification of initial conditions. That is followed by a exponential growth rate region and a saturation region.

Figures 11 and 12 show iso-vorticity lines close to the beginning of the saturation region for $c = 0.003$ and $c = 0.009$ For the heat strength considered no significant differences were observed on the thickness of the vortices. Iso-vorticity lines for the other two Mach numbers considered are similar (not shown).

Increasing the Mach number to $M = 0.6$ results in additional reduction on the amplification rates as shown in Fig. 13. For this level of compressibility heat addition has a greater effect on disturbances with higher wavenumbers. The time evolution of $v(t)$ is shown in figure 14 for different levels of heat addition, including the case of no heat addition. compared to the case $M = 0.4$ the curves are more spread apart, showing that a higher Mach number has a stronger influence on the growth rate.

Iso-vorticity lines for $c = 0.003$ and $c = 0.009$ are shown in Figs. 15 and 16 for $M = 0.6$ and $\alpha = 0.7$. Close to the point where saturation takes place, the vortices are little more elongated than at $M = 0.4$, but does not seems to vary much for the different levels of heat addition.

For a compressibility level of $M = 0.8$, again the amplification rates are reduced, as shown in if Fig. 17. But the effect on the higher wavenumber limit is stronger than the effect observed for the other compressibility levels. The range of unstable wavelengths is reduced increasing the heat strength. The simultaneous effect of compressibility and heat addition on the growth rate can be seen clearly on the temporal evolution of $v(t)$. The same levels of heat addition promotes a stronger stabilization of the shear layer if the compressibility is higher. This effect is evident also on Fig. 18 for the evolution of $v(t)$. In other words, flows with higher compressibility are more sensitive to heat addition. The iso-vorticity lines in Figs 19 and 20 show similar behaviour as for $M = 0.6$.

4. CONCLUSIONS

A higher order finite differences code was used in a direct numerical simulation of the Navier-Stokes equations to study the development of instabilities in a shear layer with heat addition. The results show that compressibility has a stabilizing effect and this effect is stronger on high wavenumber disturbances. When heat is added to the shear layer, as in a combustion process, the shear layer is further stabilized. The effect of heat addition is also higher on high wavenumber disturbances. When the combined effect of compressibility and heat addition is considered it was observed that heat addition has a stronger stabilizing effect with increasing compressibility.

5. REFERENCES

Brown, G. L. and Roshko, A., 1974, On density effects and large structure in turbulent mixing layers, "Journal of Fluid Mechanics", Vol. **64**, pp. 775–781.

Chinzei, N. G., Masuya, T., Komuro, T., Murakami, A., and Kudou, K., 1986, Spreading of two-stream supersonic turbulent mixing layers, "Physics of Fluids", Vol. **29**, pp. 1345–1347.

Clemens, N. T. and Mungal, M. G., 1995, Large-scale structure and entrainment in the supersonic mixing layer, "Journal of Fluid Mechanics", Vol. **284**, pp. 171–216.

Day, M. J., Mansour, N. N., and Reynolds, W. C., 1998, The structure of the compressible reacting mixing layer: Insights from linear stability analysis, "Physics of Fluids", Vol. **10**, pp. 993–1007.

Day, M. J., Mansour, N. N., and Reynolds, W. C., 2001, Nonlinear Stability and Structure of Compressible Reacting Mixing Layers, "J. of Fluid Mechanics", Vol. **446**, pp. 375–408.

Germanos, R. A. C. and Medeiros, M. A. F., 2005, Development of a Code for a Direct Numerical Simulation of Compressible Shear Flow Instability, "Décimo Oitavo Congresso de Engenharia Mecânica–COBEM", Ouro Preto, MG. Associação Brasileira de Engenharia e Ciências Mecânicas–ABCM.

Groppengiesser, H., 1970, Study on the stability of boundary layers in compressible fluids, Technical Report NASA TT F-12, National Aeronautics and Space Administration – NASA.

Ho, C. M. and Huerre, P., 1984, Perturbed Free Shear Layers, "Annual Review of Fluid Mechanics", Vol. 16, pp. 365–424.

Jackson, T. L. and Grosch, C. E., 1989, Inviscid spatial stability of a compressible mixing layer, "Journal of Fluid Mechanics", Vol. **208**, pp. 609–637.

Jackson, T. L. and Grosch, C. E., 1990, Inviscid spatial stability of a compressible mixing layer - Part 2 - The flame sheet model, "Journal of Fluid Mechanics", Vol. **217**, pp. 391–420.

Lele, S., 1992, Compact Finite Difference Schemes with Spectral-like Resolution, "J. Computational Physics", Vol. **103**, pp. 16–42.

Lessen, M., Fox, J. A., and Zien, H. M., 1965, On the inviscid instability of the laminar mixing of two parallel streams of a compressible fluid, "Journal of Fluid Mechanics", Vol. **23**, pp. 355–367.

Lessen, M., Fox, J. A., and Zien, H. M., 1966, Stability of the laminar mixing of two parallel streams with respect to supersonic disturbances, "Journal of Fluid Mechanics", Vol. **25**, pp. 737–742.

Mahesh, K., 1998, A Family of High Order Finite Difference Schemes with Good Spectral Resolution, "J. Computational Physics", Vol. **145**, pp. 332–358.

Papamoschou, D. and Roshko, A., 1988, The compressible turbulent shear layer: an experimental study, "Journal of Fluid Mechanics", Vol. **197**, pp. 453–477.

Planché, O. H. R., 1993, "A Numerical Investigation of the Compressible Reacting Mixing Layer", PhD thesis, Stanfor University, USA.

Quirino, S. F., 2006, "Compressible Shear Layer Direct Numerical Simulation With Heat Source", PhD thesis, Instituto de Atividades Espaciais, INPE.

Sandham, N. D., 1990, "A Numerical Investigation of the Compressible Mixing Layer", PhD thesis, Stanfor University, USA.

Sandham, N. D. and Reynolds, W. C., 1991, Three-dimensional simulations of large eddies in the compressible mixing layer, "J. Fluid Mechanics", Vol. **224**, pp. 133–158.

Sauvage, R. and Kourta, A., 1999, Compressible Effects on a Temporal Direct Numerical Simulation, de Mathématiques Appliquées et Industrielles, S., editor, "Third International Workshop on Vortex Flows and Related Numerical Methods", Vol. 7 of "European Series in Applied and Industrial Mathematics–ESAIM", pp. 378–386. Société de Mathématiques Appliquées et Industrielles.

Shin, D. S. and Ferziger, J. H., 1991, Linear stability of the reacting mixing layer, "AIAA Journal", Vol. **29**, pp. 1634–1642.

Shin, D. S. and Ferziger, J. H., 1993, Linear stability of the compressible reacting mixing layer, "AIAA Journal", Vol. **31**, pp. 677.

Souza, L. F., 2003, "Instabilidade Centrífuga e Transição para Turbulência em Escoamentos Laminares Sobre Superfícies Côncavas", PhD thesis, Instituto Tecnológico de Aeronáutica.

6. Responsibility notice

The author(s) is (are) the only responsible for the printed material included in this paper

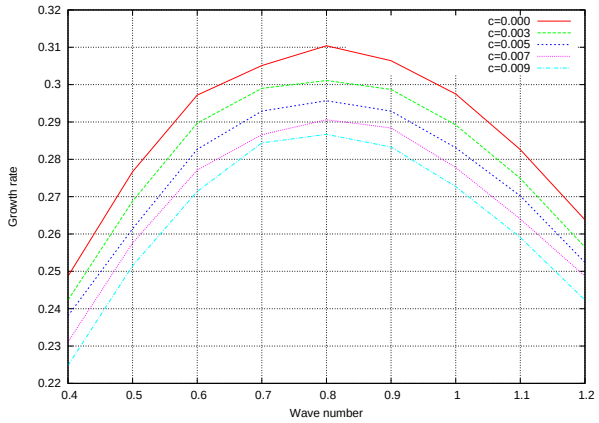

Figure 9. Growth rates for $M = 0.4$ in a shear layer with heat addition.

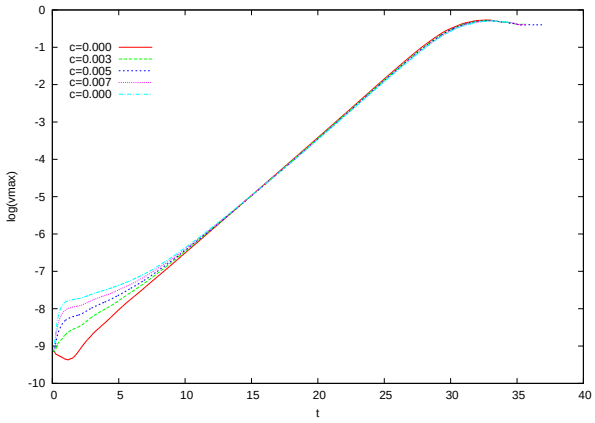

Figure 10. Maximum vertical velocity disturbance versus time for $M = 0.4$.

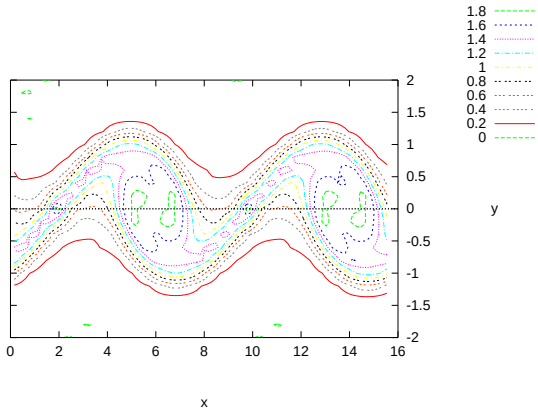

Figure 11. Vorticity iso-lines for $M = 0.4$ and $\alpha = 0.8$ for c_1.

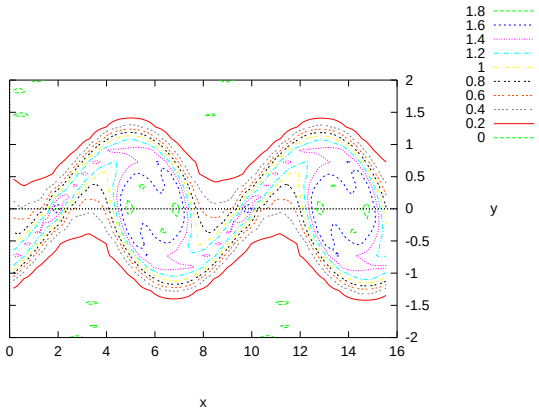

Figure 12. Vorticity iso-lines for $M = 0.4$ and $\alpha = 0.7$ for c_4.

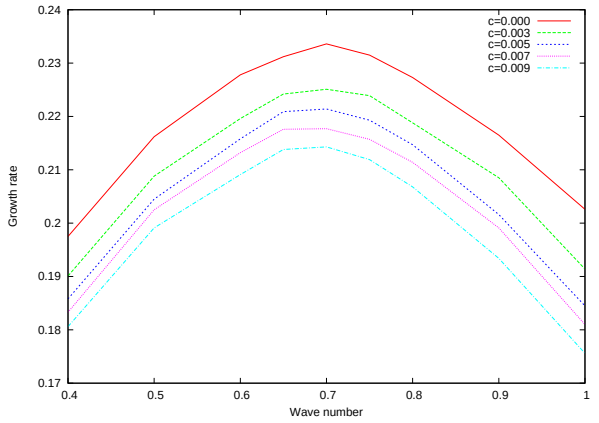

Figure 13. Growth rates for $M = 0.6$ in a shear layer with heat addition.

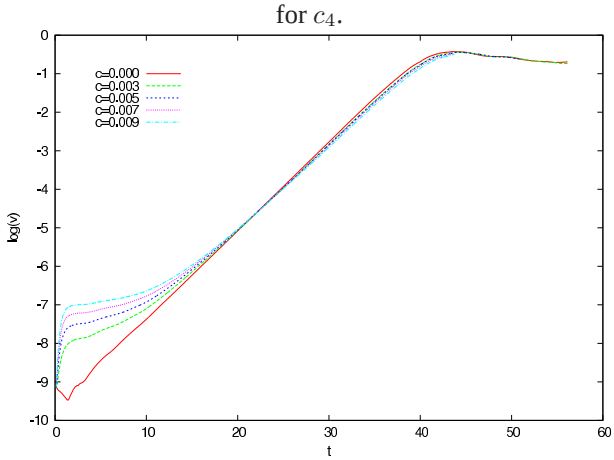

Figure 14. Maximum vertical velocity disturbance versus time for $M = 0.6$.

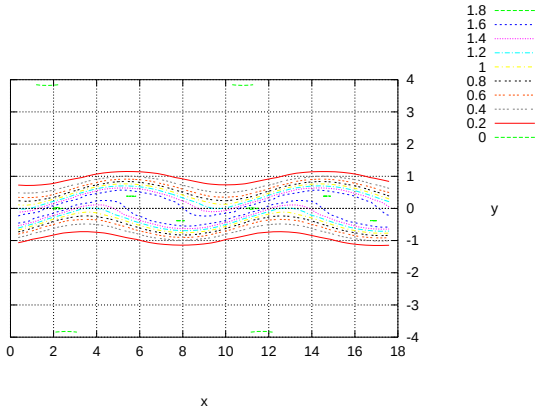

Figure 15. Vorticity iso-lines for $M = 0.6$ e $\alpha = 0.7$ and c_1 for $t = 38.92$.

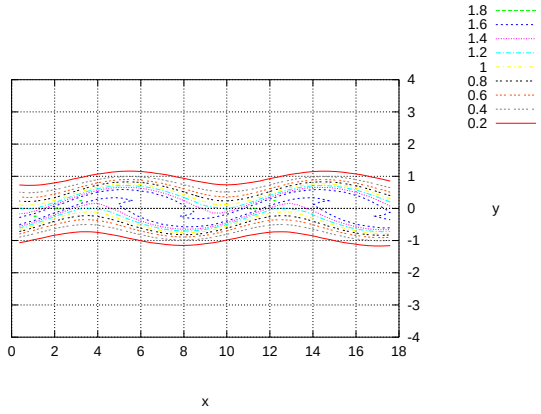

Figure 16. Vorticity iso-lines for $M = 0.6$, $\alpha = 0.7$ and c_4 for $t = 38.56$.

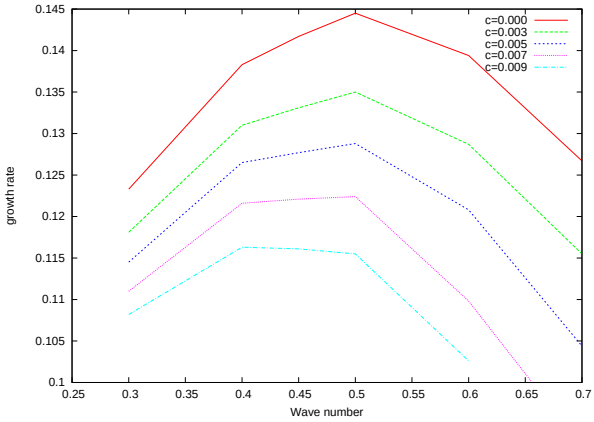

Figure 17. Growth rates for $M = 0.8$ in a shear layer with heat addition.

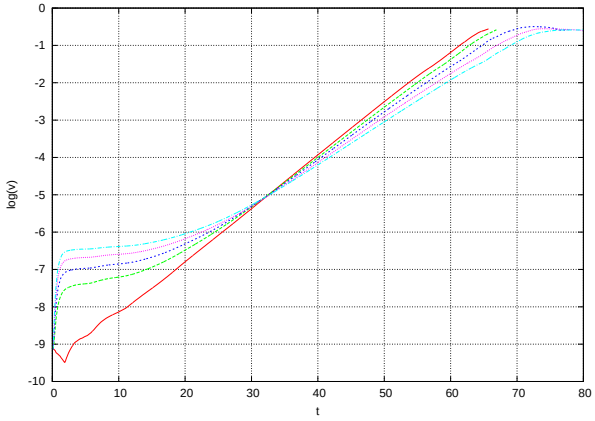

Figure 18. Maximum vertical velocity disturbance versus time for $M = 0.8$.

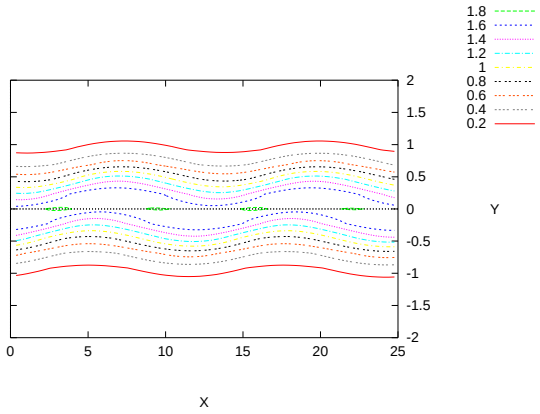

Figure 19. Vorticity iso-lines for $M = 0.8$, $\alpha = 0.5$ and $c = 0.003$ at $t = 50.33$.

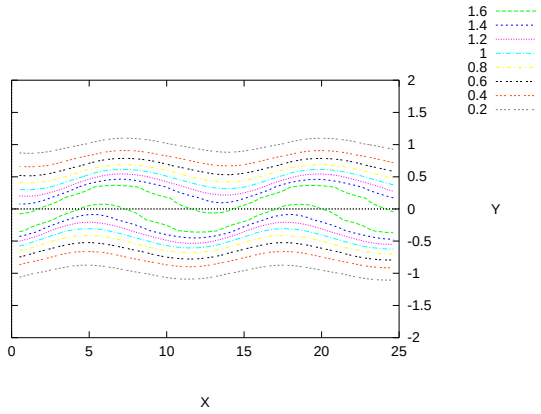

Figure 20. Vorticity iso-lines for $M = 0.8$,$\alpha = 0.5$ and $c = 0.009$ at $t = 58.34$.